Ocean Engineering
May 2020, Volume 203 Pages 107144 (12p.)
https://doi.org/10.1016/j.oceaneng.2020.107144
https://archimer.ifremer.fr/doc/00615/72668/

Influence of bedding-in on the tensile performance of HMPE fiber ropes

Bain Cédric [1, 2, 3, *] , Davies Peter [2], Bles Guilhem [1], Marco Yann [1], Barnet Julien [3]

[1] ENSTA Bretagne, Institut de Recherche Dupuy de Lome IRDL-UMR CNRS 6027, Brest, France
[2] IFREMER Centre Bretagne, Marine Structures Laboratory, Plouzane, France
[3] INO-ROPE, Concarneau, France

* Corresponding author : Cédric Bain, email address : cedric.bain@ensta-bretagne.org

Abstract :

Synthetic fiber ropes are widely used in the maritime industry, with applications from sailboat rigging to offshore platform mooring lines, thanks to their numerous qualities compared to steel cables: light weight, good specific mechanical properties and excellent marine resistance. A key feature of these ropes is their sensitivity to loading history, as this affects subsequent performance. In the present work the influence of the maximum bedding-in load level and the loading path were studied at the different rope component scales (filament, yarn and braided rope), in order to develop an optimal bedding-in procedure for braided ropes. The load levels were: 10%, 30% and 50% of the tensile break load of the sample. From the results obtained, the influence of braid construction and material have been studied, and an efficient bedding-in process has been defined. It was shown that the main parameter is the maximum load level, the loading path is not important. The load required to bed in HMPE ropes is closely related to changes in the braid angle under load.

Highlights

► Unique results of the influence of bedding in protocol on at different rope scales. ► Influence of bedding-in loading path and loading level on tensile behavior. ► Correlation between fibers reorientation and bedding-in protocols. ► Separation of contributions from material and construction.

Keywords : HMPE, Rope, Bedding-in, Stretched, Fiber, Braided

Introduction

Fiber ropes have been used for thousands of years, thanks to their excellent tensile strength, environmental resistance and light weight. Synthetic materials such as polyester, polyamide, aramid, and polyethylene are newcomers in the history of fiber ropes, and have extended the range of possible applications. They offer the potential to replace many steel wire ropes and chains, especially for mooring lines. However, synthetic fiber rope behavior is more complex than that of steel wire ropes; this is due to both the complex behavior of polymer fibers and the hierarchical structure of rope components (Leech, 2002). The most common rope construction used in mooring lines is based on twisted strands, and these have been widely studied (Del Vecchio, 1992; Ghoreishi, 2005; Raoof and Hobbs, 1988). Braided ropes are the other main type of rope construction, and have also been studied in the past decades (Davies et al., 2002; Vu et al., 2015). A bedding-in protocol, a sequence of tensile loading to settle the fibers and their geometry, is essential for synthetic fiber ropes. It allows stabilizing the mechanical properties of ropes by applying a known loading history to the rope before use. To understand the consequences of the bedding-in protocol on the rope deformation mechanisms, some researchers have focused on the influence of rope construction on the mechanical behavior (Hoppe, 1991; Leech and Hearle, 1993; Raoof and Hobbs, 1988), and others on the role of loading history (Casey et al., 2000; Davies et al., 2002; Del Vecchio, 1992). These two points concerning the construction and the history effect need further investigation.

Many investigations have focused on the understanding of the geometry of the rope, the interactions between each scale and the behavior of smaller scales, in order to be able to model numerically or empirically the mechanical behavior of synthetic fiber ropes. For example, (Ghoreishi et al., 2007) developed a nonlinear elastic continuum model based on various earlier models for steel and synthetic stranded ropes such as those of (Hoppe, 1991; Leech and Hearle, 1993; Raoof and Hobbs, 1988). These models are based on the geometries and the properties of each scale, and friction is also considered in some of them. (Davies et al 2006) applied Leech's model and found a good correlation of tension/torsion properties for results on full size long rope samples. Braided ropes have received less

attention than stranded ropes, but some researchers have investigated behavior models, in particular (Rawal et al., 2015; Vu et al., 2015). The development of finite element simulations and other analytical models are helpful to understand the complex behavior of fiber ropes and the mechanisms of the bedding-in process. These must account for internal friction between fibers and the reorganization of fibers under the load.

The bedding-in process and loading history effects have been studied in some detail during the development of the use of polyester ropes for floating platform mooring lines in the offshore industry. It is generally agreed that a bedding-in process will change the mechanical properties of ropes significantly. For (Banfield and Casey, 1998) the bedding process has to be recorded to interpret rope properties correctly. Work by (Casey et al., 2000; Davies et al., 2002; Del Vecchio, 1992; Hooker and Bosman, 1999; Liu et al., 2014; Weller et al., 2014), has led to the conclusion that the mean load and the strain amplitude are the two main parameters which influence the mechanical behavior of ropes under cyclic loads. As (Casey et al., 2000) concluded, the dynamic stiffness after a full bedding-in process remains constant. However, if the permanent strain, due to molecular rearrangement in the fibers and geometric construction changes, is not removed by the bedding-in sequence it will result in lower stiffness values. By understanding the effects of the bedding-in, simplified behavior models for ropes can be proposed; (Davies et al., 2002) developed an empirical expression for evaluating the dynamic stiffness of HMPE ropes. (Liu et al., 2014) further developed these expressions in order to obtain the dynamic stiffness from small size ropes and extrapolate to larger ones, and also to take into account the mean load, strain amplitude and number of loading cycles. (Lian et al., 2018a) concluded that different bedding-in levels can cause different values of strain, initial creep and dynamic stiffness for the same test samples. For this reason the investigation of the bedding-in behavior of synthetic fiber ropes is essential for most applications. Even if there is agreement on the need for a bedding-in procedure to stabilize rope behavior before measuring stiffness values, there are different recommendations: (American Bureau of Shipping (ABS), 2011; Bureau Veritas, 2007; International Standards Organization (ISO), 2004). Bedding-in protocols are not the same according to each guideline, but they have the same purpose, which is to stabilize the rope length and to improve rope and termination efficiencies. (Del Vecchio, 1992) used a bedding-in loading sequence of 1000 cycles between 10% and 30% of the minimum breaking load (MBL).

(Casey and Banfield, 2005) concluded that at least 10000 cycles are required to get nearer to a fully bedded-in state, but they recommend that at least 500 cycles be applied. (Lechat, 2007) followed a recommendation of the Oil Companies International Marine Forum (OCIMF) for bedding-in before testing which includes five steps of 5min at 50% of the MBL (minimum break load) each followed by a recovery step at 2% of the MBL. (Humeau, 2017) applied 5 cycles between 2% and 50% of the MBL. These different studies show how numerous bedding-in sequences are used and that there is not a unified procedure. That is why (Lian et al., 2018a) presented a quantitative method for determining the bedding-in level of synthetic fiber ropes based on the tension-strain curve for static tensile loading. The permanent elongation (Francois and Davies, 2000; Humeau, 2017) of synthetic fiber ropes is the result of two types of elongation: the rope construction component and the material contribution. The permanent elongation related to the construction can be explained by compaction and the realignment of fibers in the loading direction. (Chailleux and Davies, 2005; Humeau, 2017; Williams et al., 2002) have included these contributions in elasto-viscoelastic-plastic models, which they applied to polyester and aramid yarns. (Williams et al., 2002) have observed that for a basic response for each sub-scale, the response of the rope is not the same due to the construction influence.

Most of the published work on bedding-in has been focused on polyester, polyamide and aramid fibers. Very few authors, with the exception of (Costa and Chimisso, 2011; Davies et al., 2011; Humeau et al., 2018; Lian et al., 2019, 2018b, 2015) have considered HMPE. To the authors' knowledge no previous studies have presented results for ropes based on the Dyneema™ SK99 HMPE grade. This grade was specially developed for the nautical industry and shows high tensile stiffness and strength. Table 1 shows nominal properties of different grades of Dyneema™ (Vlasblom, 2018). There are also few published test results from tests at different scales of a rope construction, and these are essential in order to establish the influence of load history on each one. In the present study different input parameters have been varied, such as maximum load during bedding-in; this has been done previously, but here the loading history path was also varied in order to understand its contribution.

In summary, bedding-in is primordial for synthetic fiber ropes, and a thorough understanding of the mechanisms involved is very important for many marine applications. For example, neither tensioning of sailboat rigging nor the installation of offshore mooring lines is possible without a good estimation of

elongation during first loading. The aim of the present study is to separate the construction and material contributions of the bedding-in process to the mechanical behavior of HMPE braided ropes. Different bedding-in sequences will be applied to investigate the influence of the loading history on the mechanical behavior. First, the material and experimental devices will be presented, followed by the definition of the bedding-in protocols. The stress-strain curves from static tensile tests for each scale of synthetic fibers ropes will then be presented. Based on the test results, the discussion will provide conclusions about the optimal bedding-in process and the influence of rope construction.

HMPE Grade	Filament Diameter (µm)	Filament Linear Density (denier =g/9000m)	Yarn Linear Density (tex)	Tensile Strength (N/tex)	Tensile Modulus (N/tex)	Elongation to break (%)
SK99	12	1.0	88	4.3	159	3.5
SK78	17-21	2.0-3.0	176-264	3.4-3.5	112-116	3.5
SK75	17-21	2.0-3.0	5.5-264	3.4-4.0	112-138	3.5
DM20	17	2.0	176	3.2	96	

Table 1. Properties of the different grades of Dyneema from (Vlasblom, 2018)

I. Materials and Methods

a. Material

The synthetic fiber ropes tested in the present study were made of Dyneema™ SK99 fibers. The rope was braided with a 16-strand construction and a nominal diameter of 4mm. A coating was applied by the manufacturer. The samples were provided by the Lancelin Corderie (Ernée, France). The results from these small diameter ropes can be used as a first approach towards understanding the behavior of bigger ropes, such as the ones used in offshore platform mooring lines.

As many researchers have shown previously, the geometrical structure of the rope is one of the major factors in determining the mechanical elongations that occur during bedding-in process. In order to

quantify the importance of the construction, the study investigated the bedding-in behavior at different rope levels, Figure 1.

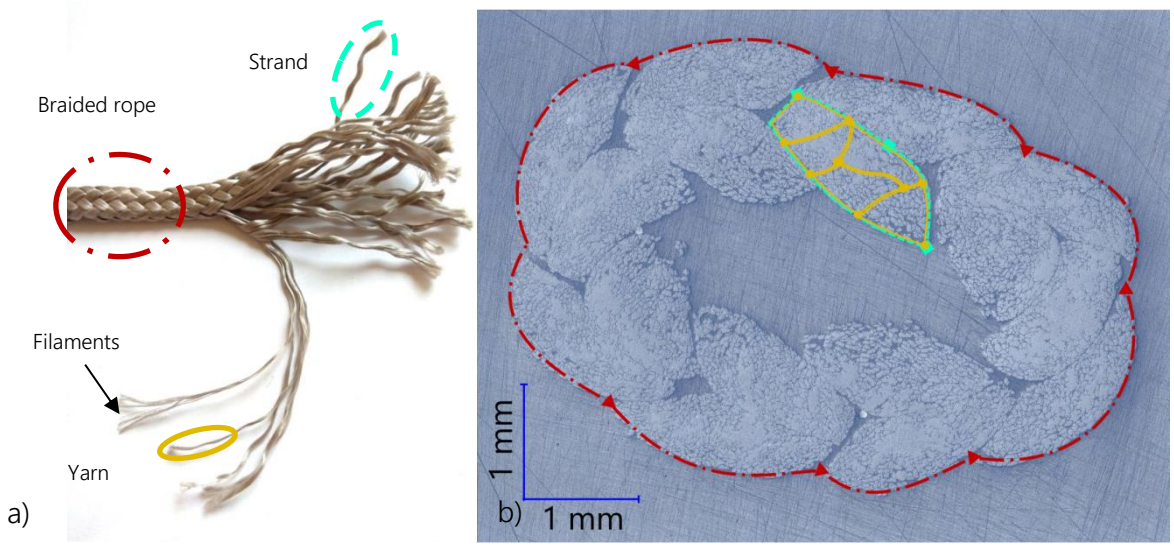

Figure 1. a) The studied braided rope and its components, b) section through new rope before loading, showing strands, yarns and filaments.

The different scales are the braided rope, the strand, the yarn and the filament. The rope is made of 16 strands, each strand composed of 5 yarns and each yarn of approximately 800 filaments.

b. Samples and Experimental Equipment

i. Rope

The tensile testing machine used for ropes is an ADAMEL™ Lhomargy DY 36 with a 100kN load cell.

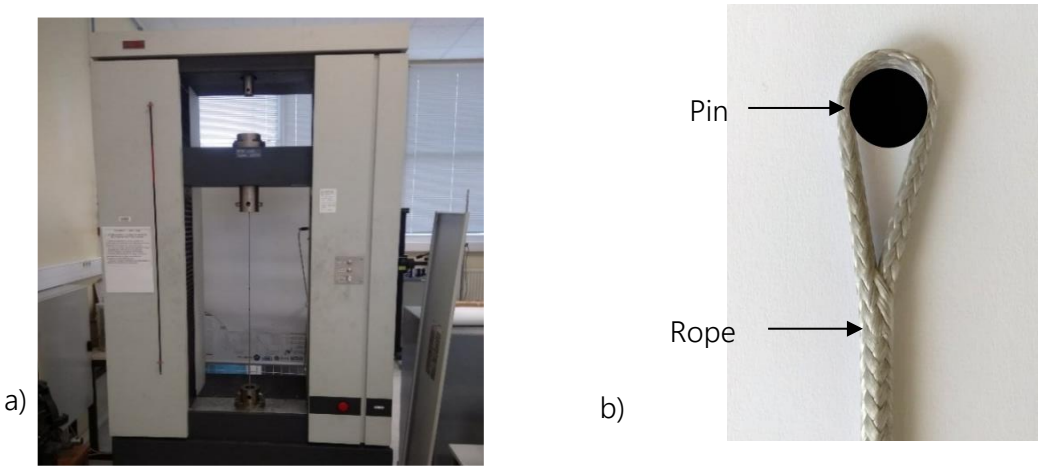

Figure 2. a) Rope sample on test machine and b) attachment method by splice.

The 100kN load cell was calibrated in 2019. It has an accuracy of +/-5.8N (+/-0.0421%) for a 14kN load.

The test specimens are ropes with eye splices at each end, Figure 2. Several researchers (Leech, 2003;

Leech and Hearle, 1993; Milne and Mclaren, 2006) have studied the best way to terminate a braided rope, and eye splices provide the maximal strength. Rope samples were loaded with steel pins with a diameter of 20mm.

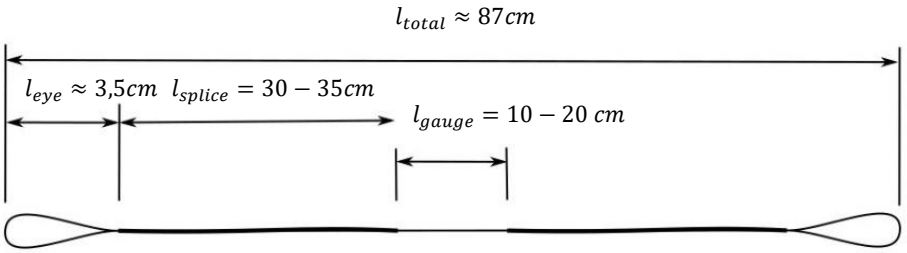

Figure 3. Rope sample geometry.

A local strain measurement system was used in order to avoid measuring the slip that will occur in the end termination during loading. For the case of the rope, a RETIGA 6000 camera and NI Vision Assistance software allowed the movement of two markers, fixed to the rope, to be followed.

Each rope sample was weighed and its length measured before making the splices, in order to determine its linear density.

The initial dimensions of the rope samples were 10-20 cm of usable length in the central section, l_{gauge} , each splice length l_{splice} measured 30-35cm with an eye length around 3.5cm, giving a total length l_{total} of 87 cm, Figure 3.

Break loads were also determined: Eight monotonous loading tests until failure were performed to obtain a mean breaking load. The mean loading rate was 1%/min. The mean rope breaking load obtained was 14.7kN, with a standard deviation of 786N.

The linear density of the rope was measured and a value of 8.685 g/m was obtained.

Despite the fact that the strains are measured directly in the gauge region, the vicinity of the splices may have an effect on the strain measured. To investigate the influence of the distance from the splice on the strain measured, additional tests have been performed on a Dyneema SK99 rope with a diameter of 4mm, as shown in Figure 4. Figure 5 represents several markers which were located at different lengths from the end of a splice.

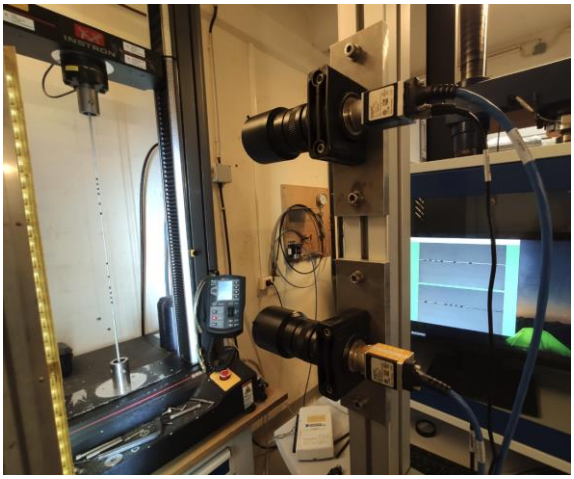

Figure 4. Monotonous loading on rope with different markers

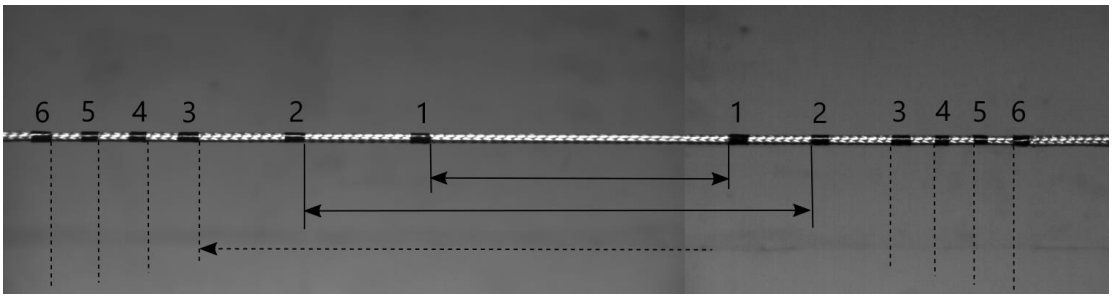

Figure 5. Location of the markers

The marker noted '6' is located directly over the end of the splice, while 1, 2, 3, 4, 5 are located at different distances away. The overall gauge length, between the two end splices is 388mm.

In order to observe the influence of the splices on the measured strain, different stress-strain curves are plotted.

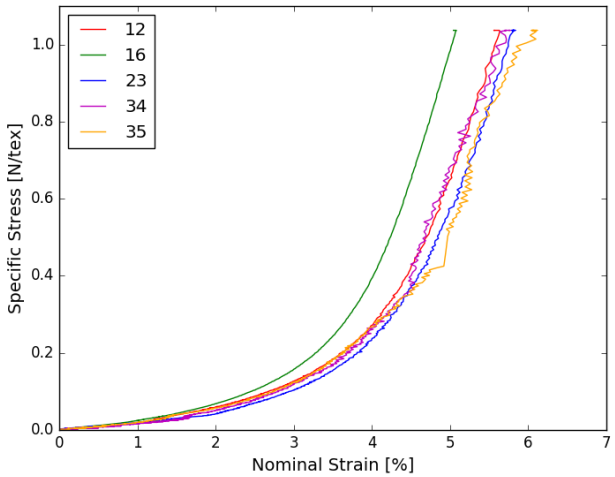

Figure 6. Stress-Strain results for different markers

Figure 6. shows the influence of the marker position on the measured strain. When measurements are made directly from the end of the splice a stiffening effect is noted (curve 1-6), whereas measurements away from the splice end (the other 4 curves in Figure 6) provide very similar stress-strain plots, within experimental scatter. Thus the strain field is certainly affected by the splices but provided markers are placed even a small distance away (as was the case for the values shown in this paper) the influence on measured strain is small. These are results from only one test but they do indicate that strain field is uniform over most of the gauge length.

ii. Yarn

The test machine used for yarns was an INSTRON model 5566, with a 500N load cell, Figure 7.

a)

b)

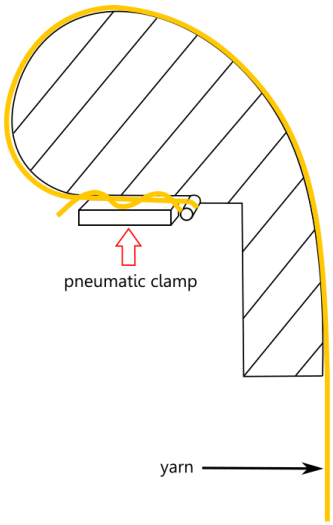

Figure 7. Yarn sample on test machine (a) and attachment method (b).

The experimental setup is similar to the one used for the rope. Each marker was followed by a camera to determine the local deformation. Special pneumatic clamps were used to grip the samples, as shown in Figure 7.b).

Yarns were extracted from the braided ropes. The coating applied on the yarns makes separation of the strand into five yarns straightforward.

In the same way as for the ropes, the mean breaking load of the yarns was measured on 10 samples to be 277N (with a standard deviation of 10.1N). The mean loading rate was 0.169 %/min. Linear density was measured to be $9.73.10^{-2}$ g/m, the gauge length of samples was 250mm.

iii. Filament

The same INSTRON 5566 test machine was used for filaments, but with a 50N load cell. This load cell was calibrated in 2018. Its accuracy is of +/- 0.0021N for a 1N load. Therefore for a MBL of 0.402, the relative uncertainty is of +/-0.5%.

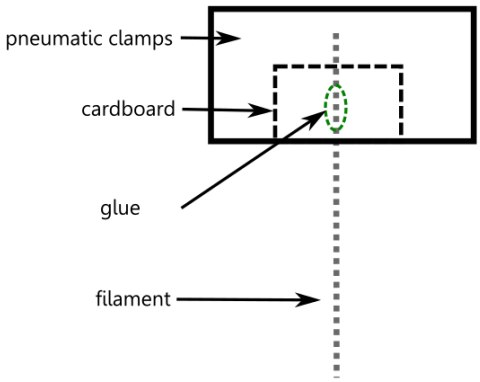

Figure 8. Attachment method for filament samples.

The filaments were extracted from the yarns. After extraction of the filament, each end of the latter was adhesively bonded between two pieces of cardboard. Pneumatic clamps were used to grip the cardboard (cf. Figure 8).

In order to determine the linear density of the filament, the section of a yarn was first observed by digital microscopy (KEYENCE™) to count the number of filaments. The linear density of the filament was then determined as follows:

$$\rho_{filament} = \frac{\rho_{yarn}}{number\ of\ filaments\ in\ a\ yarn}$$

The difficulty of filament extraction and the very small filament diameter make fixing markers to the specimen difficult. Several preliminary tests were performed with local markers and these showed that

there was no slip in the clamps. For subsequent tests, the clamp movement was therefore used to measure the filament strain.

In the same way as for the ropes, the mean breaking load of the filaments was measured to be 0.402N (12 samples with a standard deviation of 0.059). The mean loading rate was 5%/min. Linear density was $1.24.10^{-4}$ g/m, the gauge length of filament samples was around 95mm.

c. Definitions and Protocols

i. Parameters

Figure 9 shows the parameters studied here.

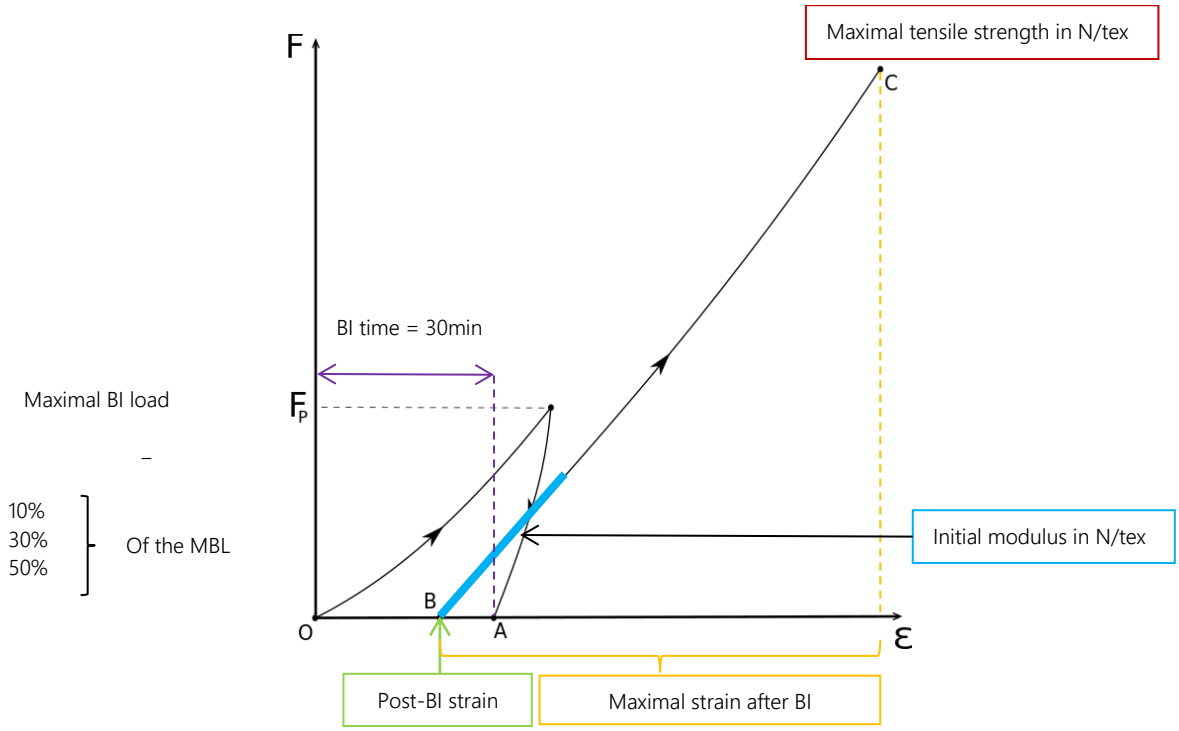

Figure 9. Extracted data for the case of load/unload bedding-in (BI) protocol.

ii. Stress and Strain

As noted previously, synthetic fiber ropes have complex structures. The Cauchy stress based on the sample cross-section will be difficult to use in this study. A specific stress $\tilde{\Sigma}$ (Costa and Chimisso, 2011; Fer, 1971), is preferred, which is based on the linear density of the rope:

With:

$$\tilde{\Sigma} = \frac{1}{\rho_t}\tilde{T}$$

With:

- ρ_t : density in kg/m^3
- $\tilde{T}$: Cauchy stress tensor in Pa

In the 1D case (rope case), this specific stress leads to:

$$\Sigma = \frac{F}{\bar{\bar{\rho}}}$$

With:

- $\bar{\bar{\rho}}$: linear density in kg/m
- F: Tensile Force in N

The S.I. specific stress unit is N.m/kg or J/kg. In 1D case, an equivalent unit is preferred, N/tex:

$$1\ \frac{J}{g} = 10^{-3}\ \frac{N}{tex} = 1\ \frac{Pa}{\left({}^{g}/_{m^3}\right)}$$

Where $1\ tex = 1\ g/km$.This specific stress will allow a comparison between the behaviors at each rope scale.

The nominal strain ε will be used for this study:

$$\varepsilon = \frac{\Delta l}{l_0} = \frac{l - l_0}{l_0}$$

With:

- l_0 : Initial length
- l : current length

For each scale, the detailed experimental procedure will be described.

iii. Bedding-in Protocols

Three bedding-in protocols were studied: 1 cycle (load/unload), 10 cycles (load/unload) and relaxation. On figure 7, the loading path of each test sequence is plotted. After each of these tests, a 1-hour recovery step was applied, in order to remove the visco-elastic behavior resulting from the previous load.

The effects of bedding-in maximal load are investigated. The different bedding-in maximal loads were chosen as follows, based on the industrial use of this type of rope: 10%, 30% and 50% of the MBL (Mean Breaking Load) HMPE rope. Most guidance notes for synthetic fiber ropes recommend a maximal

bedding-in load of 50% of the MBL of the rope. However, for large diameters or very long ropes such as mooring lines, test machines may not be able to reach this level. For this reason investigations into the effects of lower maximal loads for a bedding-in protocol are important.

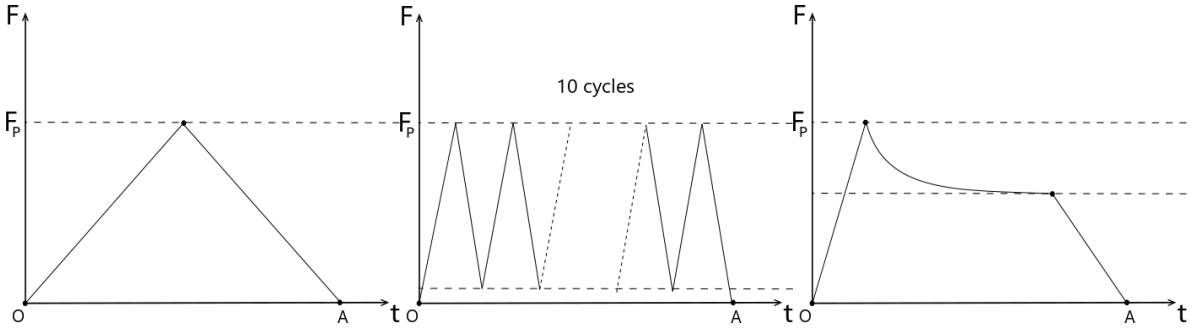

Figure 10. Bedding-in protocols studied

As shown in Figure 10, the different paths between point O and point A describe the different types of bedding-in chosen here. The time between these two points is the same for each type of bedding-in, in order to avoid any bias from visco-elastic effects. Also the relaxation time is the same as the time to perform 9 load/unload cycles.

These bedding-in protocols were applied to the different components of the HMPE rope: the filament the yarn, and the rope itself. Due to the difficulty in keeping the strand together after extracting it from the rope, that scale was not tested.

After the 1h recovery following the bedding-in protocol, a monotonous uniaxial loading up to failure was applied to the specimen to characterize its mechanical behavior. The extracted data were: the initial modulus E_i, the maximal tensile strength, the post bedding-in strain, and the maximal strains without and after bedding-in protocols (Figure 10).

Henceforth in this study, the bedding-in protocols will be called BI protocols, and simplified by the following acronyms:

- LU : one Load/Unload
- 10cLU : 10 cycles Load/Unload
- R : load, Relaxation and unload

The optimum bedding-in protocol has several criteria to satisfy:

- Be fast
- Minimize bedding-in loading level (particularly for large ropes)
- Stabilize the mechanical response by eliminating the construction effect
- Introduce no damage (No reduction of the maximal stress).

II. Results

a. Results without BI

Figure 11 shows the tensile test results without any bedding-in.

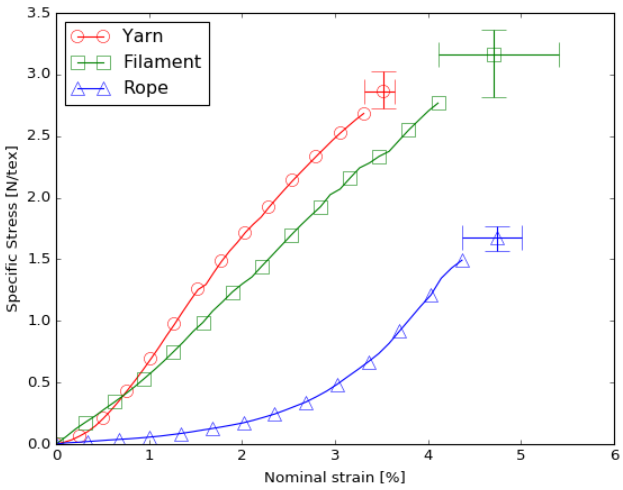

Figure 11. Monotonous loading without BI for each scale of the rope

Each of the curves is the mean of 3 test samples. The last point with the error bar shows the break point with the minimum and the maximum of the nominal strain and specific stress from the three tests.

b. Results with BI

In Figure 9, the influence of the BI load level on the rope behavior is shown. Mechanical responses of the rope during monotonous loading are plotted with and without a BI protocol.

The following figures present the mean data from the experimental bedding-in procedures described previously.

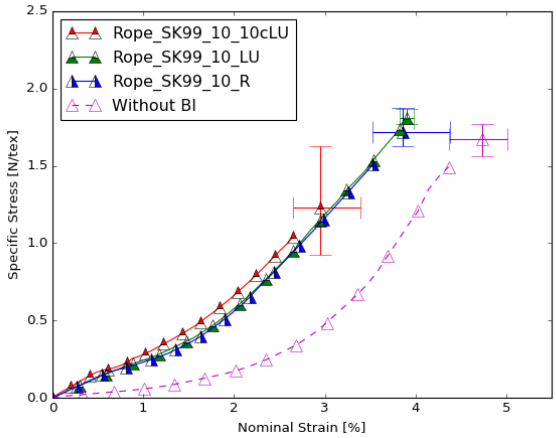

Figure 12. a. Rope results for a maximal BI load of 10% of the MBL.

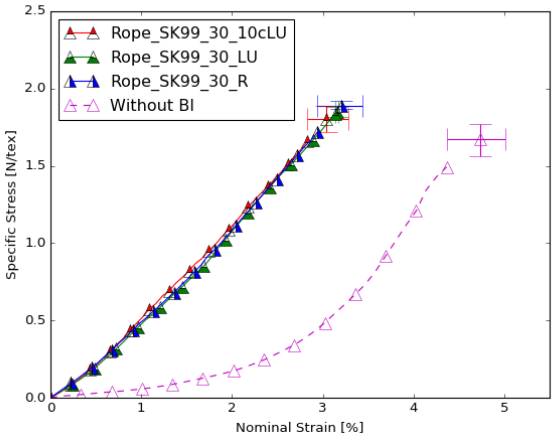

Figure 12. b. Rope results for a maximal BI load of 30% of the MBL.

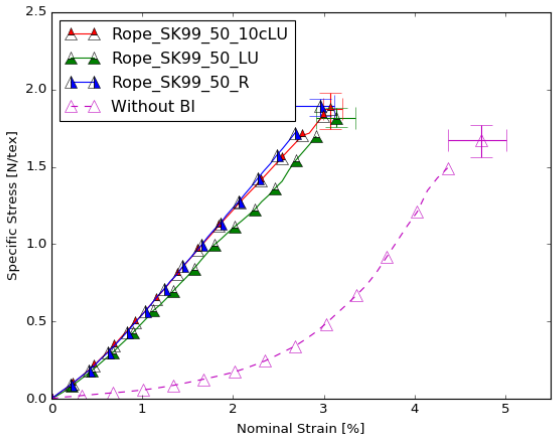

Figure 12. c. Rope results for a maximal BI load of 50% of the MBL.

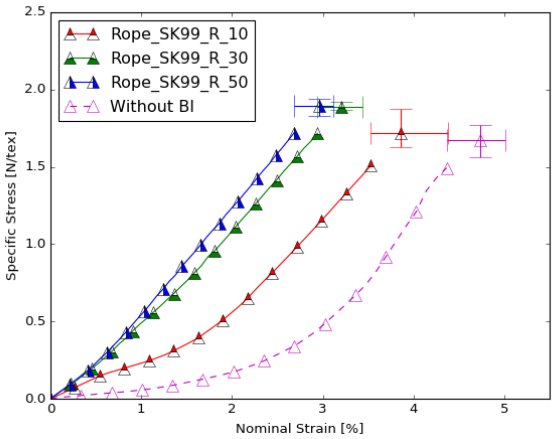

Figure 12. d. Rope results: comparison between a maximal BI load of 10%, 30% and 50% for Relaxation BI.

These figures show the strong influence of bedding-in on the subsequent mechanical behavior of the braided rope. The BI load level also has an important role. The stress-strain curves after BI, at 30% and 50%MBL load levels, are very close and mostly linear. The stress-strain curves after BI at 10%MBL load level, are between the without-BI curve and the 30-50%MBL curves. The behavior after 10%MBL BI is not linear. This shows the gap between the samples with and without BI loading.

The results in Figure 12 show that the subsequent tensile behavior of the rope after BI sequences 10cLU, LU, and R, is almost the same; this means that the loading path is not important. The main parameter is the maximal load in Figure 12.d.

c. Comparison

In this section, the effects of each of the different bedding-in protocols will be compared for each scale (rope, yarn, and filament). Figure 13 presents the corresponding results. The use of a specific stress allows the different scales to be compared directly.

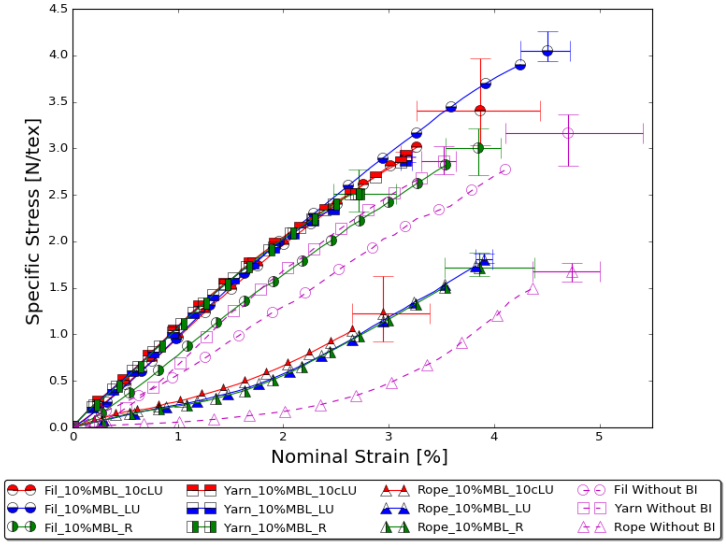

Figure 13.a. Tension after 10%MBL BI

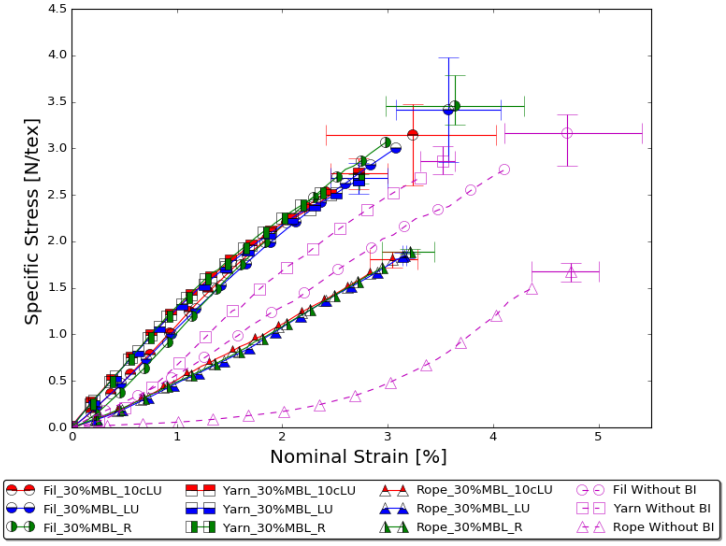

Figure 13.b. Tension after 30%MBL BI

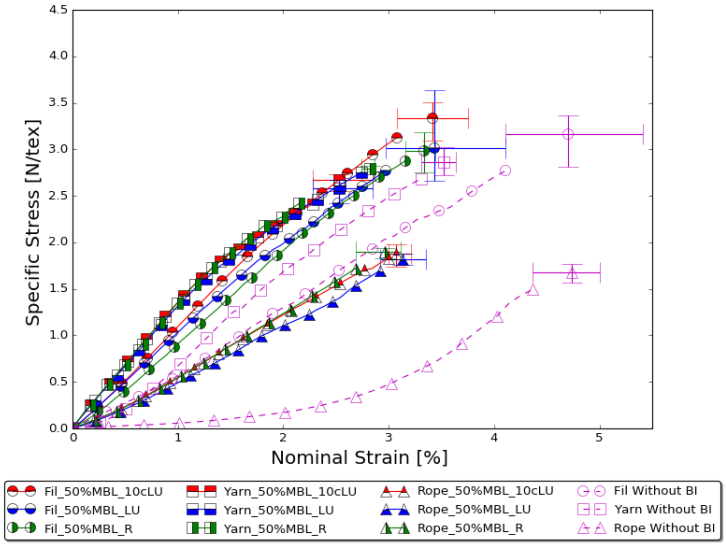

Figure 13.c. Tension after 50%MBL BI

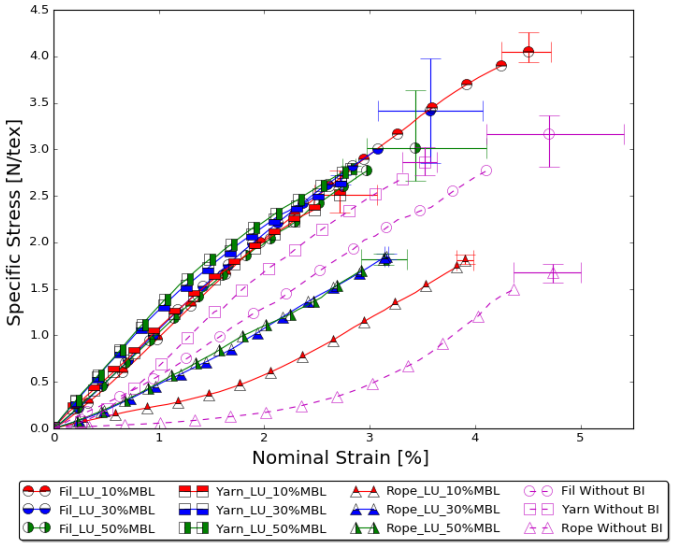

Figure 13.d. Tension after Load-Unload BI

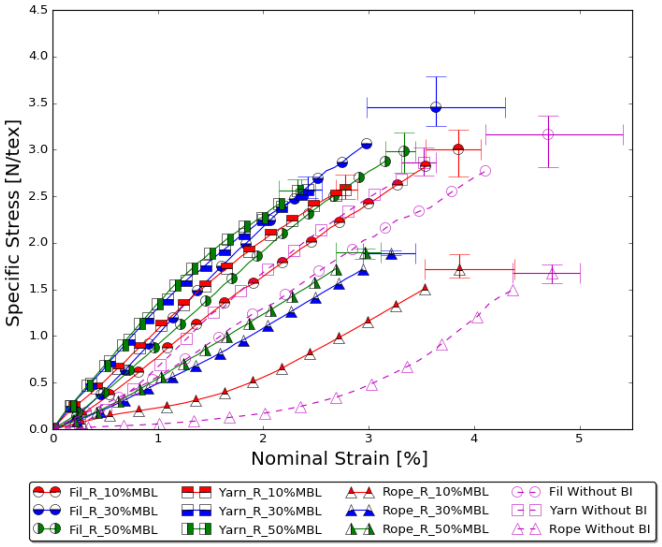

Figure 13.e. Tension after Relaxation BI

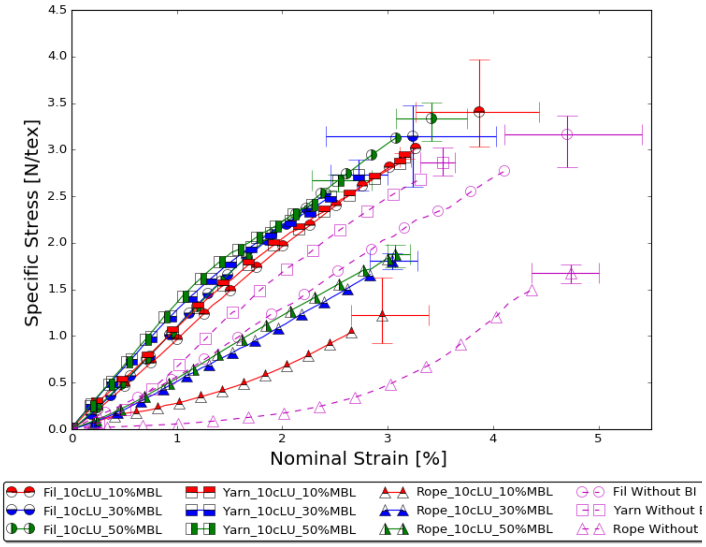

Figure 13.f. Tension after 10 load/unload cycles BI

Scales	BI Loading Level in % of MBL	Post-BI Strain in % for LU	Post-BI Strain in % for Relax	Post-BI Strain in % for 10cLU
Filament	10%	0,17	0,45	0,52
	30%	0,4	0,81	0,9
	50%	0,7	1,42	1,05
Yarn	10%	1,01	0,97	1,06
	30%	1,25	1,13	1,32
	50%	1,41	1,4	1,46
Rope	10%	1,84	1,93	2,11
	30%	2,56	2,84	2,95
	50%	2,97	3	3,71

Table 2. Post-BI strain for each BI and each scale

The post bedding-in strain is the strain due to the bedding-in loading (cf. post-BI strain description at figure 6). Table 2 shows these results for all bedding-in and all scales.

Scales	Linear density in tex	Maximal Specific Stress Without BI, N/tex

Filament	0.00124	3.16
Yarn	0.973	2.86
Rope	8685	1.67

Table 3. Maximal Specific Stress for the three scales

In Table 3, the linear densities and corresponding maximum specific stress are presented.

III. Discussion

a. Behavior of the rope and its components

i. Post bedding-in strain

The same relative classification of the post bedding-in strain for each BI was expected. It has been observed previously (Davies et al., 2006; Humeau, 2017; Liu et al., 2014) that the rope's construction influences the bedding-in behavior. The fact that filament post bedding-in strain is not zero shows that the material (fiber) history also influences the global behavior.

Scanning Electron Microscopy (SEM) observations were made on SK99 filaments (Figure 14). The coating is visible, and is not continuous along the filament. Fibrils can also be observed; these fibrils are a subscale of the filament microstructure. Different interpretations of the filament post bedding-in strain can be made. The first is to conclude that fibrils are being reoriented along the tension axis during the process. After the reorientation of the fibrils, a permanent post bedding-in strain occurs. The second possibility is that we assume that the fibrils are perfectly oriented along their neutral fiber; the post BI strain is then due to perfect plasticity of the material. The third and the most likely hypothesis is a combination of these two possibilities, which several studies have assumed (Davies et al., 2011). To verify this assumption, similar experimental tests would need to be performed at the fibril scale, but this would require very delicate measurements.

Whatever the scale, the post-BI strain increases with increasing BI load level. According to the third assumption, this plastic strain ε_p measured at the end of the recovery step is the sum of a geometrical plastic strain ε_{pg} and a material plastic strain ε_{pm}:

$$\varepsilon_p = \varepsilon_{pg} + \varepsilon_{pm}$$

The geometrical plastic strain ε_{pg} is due to the reorganization of fiber sub-scales for the case of rope, yarn and filament. And the material plastic strain ε_{pg} is due to an irreversible molecular rearrangement. For the rope case, its fiber structure being more complex, the post-BI strain is increasing more than for the yarn and the filament. The material behavior and the rope's structure are both important for stabilizing the behavior of HMPE fiber ropes.

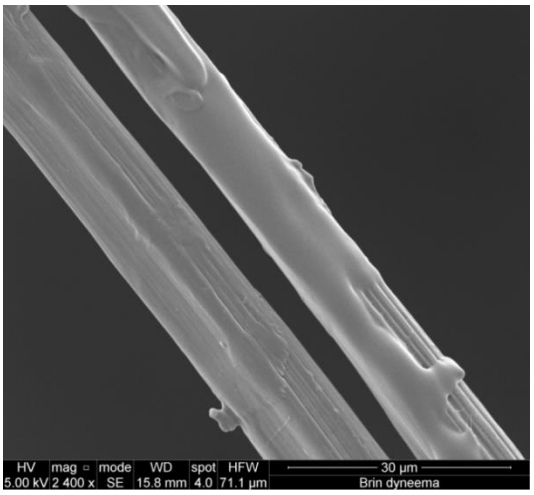

Figure 14. Two SK99 filaments

ii. Maximal strain

The maximum strain is highest for the rope scale, whatever the BI protocol. The complex assembly of fibers increases the strain due to the rearrangement of the structure of fibers. Also the maximal strain is similar for the scale of filament and yarn. This is because the filaments within the yarn are nearly perfectly aligned in the loading direction. The BI protocol reduces the maximum strain significantly.
An interesting observation is that the maximal strain is higher for the filament. The fibrils orientation in the filament may change during the filament extraction. The fibril misalignment caused by the filament extraction will disappear by stretching in the load direction and thus increasing the modulus together with the maximal tensile strength and the maximal strain.

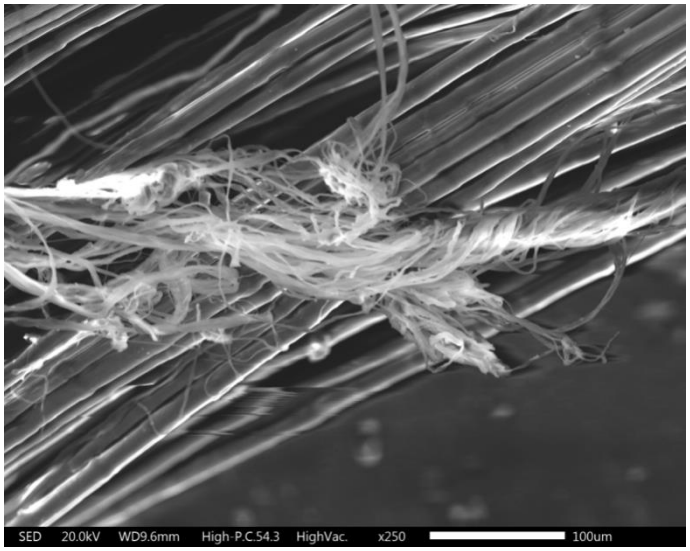

Figure 15. SEM image of extracted Dyneema filaments

iii. Initial modulus and rope behavior

The modulus values obtained here were lower than those given by the fiber producer, from 110N/tex for the filament to 136.8N/tex for the yarn compared with 159N/tex for DSM (Vlasblom, 2018). There is a difference of 14% between the yarn experimental value and the manufacturer's modulus. DSM indicates a yarn linear density in the range 80-88 tex. The linear density measured for the yarn here is 97 tex, that is 9 to 18% higher than the manufacturer's values. This difference can be explained by the presence of the coating on the filaments for the present tests, that increases the linear density. If this difference is taken into account then the experimental initial modulus values obtained for the yarn are in the same range as those of the fibre supplier. The initial modulus values for filament and yarn are at least twice as high as that of the rope. This can be explained by the effect of the construction, the fibers in the rope are stretched in the direction of the tension, but they are not in uniaxial tension. Due to the braided construction the sub-elements will be initially off-axis before reorientation of the rope occurs during tension as shown in Figure 16.

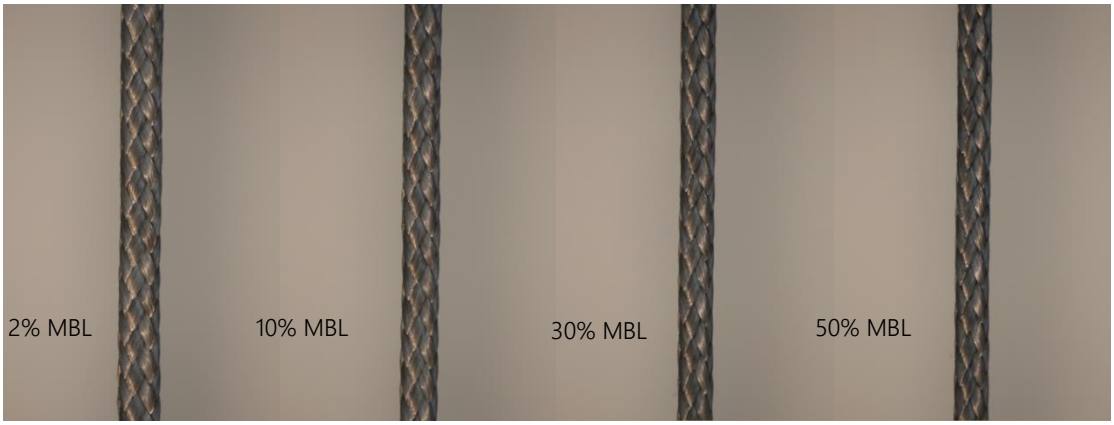

Figure 16. Images of the evolution of the rope's width during tension loading for Dyneema SK99 rope with a diameter of 4mm

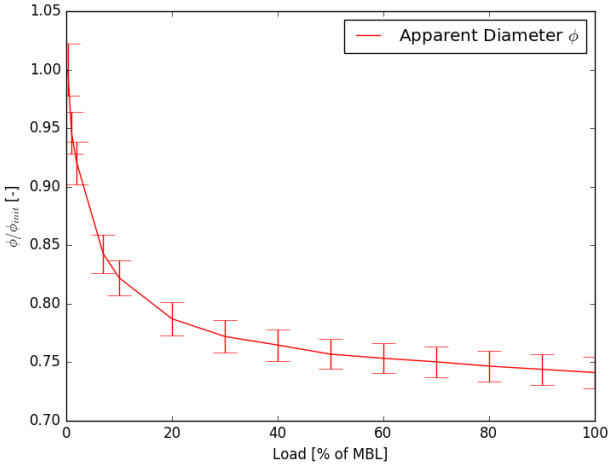

Figure 17. Change in the apparent diameter with tension loading. Error bars show standard deviation.

Figure 17 shows that the apparent diameter of the rope is decreasing significantly until 30% of the MBL and then stabilizes. The angle α between the strands was determined (cf. Figure 18). This shows the reorientation of the strands towards the rope axis. The evolution of the apparent diameter and the angle α were obtained during monotonous tensile tests on rope samples with a digital camera, which allowed the changes to the rope structure to be quantified on the recorded images using image analysis software.

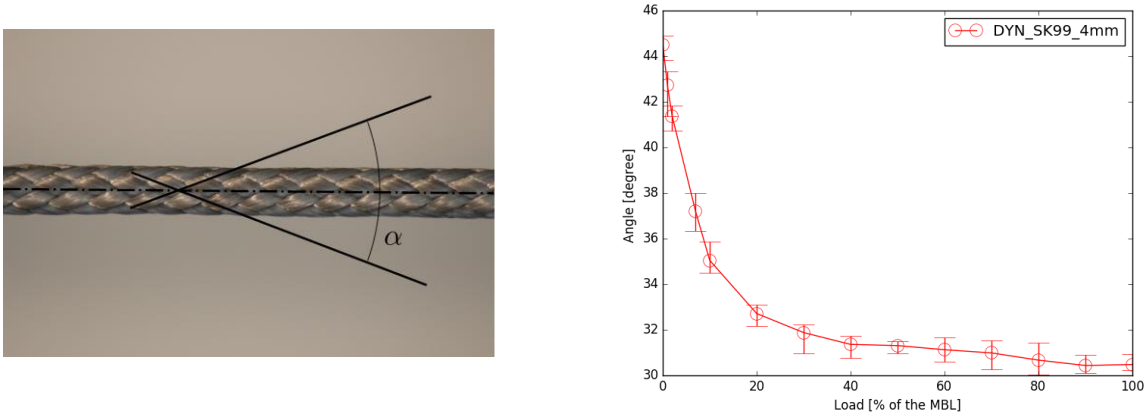

Figure 18. Change in the angle α between strands during tension loading for Dyneema SK99 rope with a diameter of 4mm. The error bars correspond to the minimum and the maximum angle measurements.

The reduction of the apparent diameter changes in a very similar way to the angle between strands and the neutral fiber of the rope, as shown in Figure 19. Also the plots become horizontal, characterizing a locking angle. This angle can be estimated from image analysis to be around 31 degrees, and corresponds to a reduction in the apparent diameter of 25%. The relationship between the lay angle of twisted ropes and their mechanical response is well known, but for braided constructions there is no simple expression (Vu et al, 2014). There appears to be a correlation here: Figure 16 shows both the maximal strain drop after different BI load levels and the evolution of the angle between strands and neutral fiber for the same loading. The similarity in the curves indicates that if the geometry is known then the mechanical behavior can be predicted. This suggests that a simple observation of the structural change of the rope during loading can indicate the optimum bedding-in loading level to reach in order to stabilize the mechanical properties of the rope. This is an interesting observation, and further investigation is needed to determine whether it is applicable for other types of rope (material, construction, diameter,...) in order to extend this conclusion.

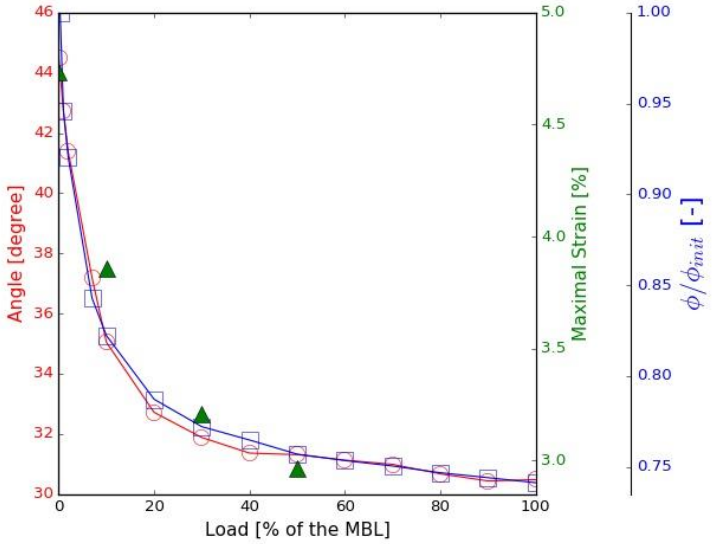

Figure 19. Evolution of the maximal strain after BI at different load levels (triangle), the apparent diameter (square) and the evolution of the angle between strands with loading (circle).

As a first step, the evolution of the angle α during a monotonous loading has been measured on two other ropes which are:

- A Dyneema SK78 16-strand braided rope with a diameter of 4mm with a MBL of 11.2kN. The construction and coating are very similar to the main SK99 rope of this study.
- A Dyneema SK78 12-strand braided rope with a diameter of 22mm and a MBL of 274kN.

An exponential function was used to fit the experimental data as follows:

$$f(x) = ae^{-bx} + \alpha_{lock}$$

With:

- a and b constants
- α_{lock} constant which represents the locking angle

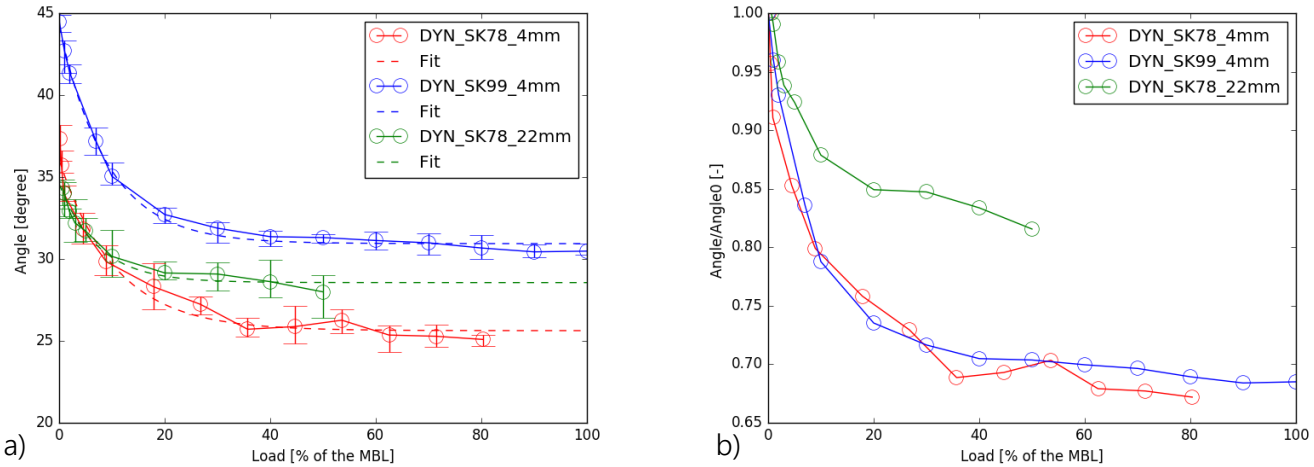

Figure 20. Evolution of α for the different rope

The optimization algorithm used for this fitting was a polynomial least squares routine. Then with this method, the locking angle is 30.9° for the Dyneema SK99 rope with a 4mm diameter, 25.6° for the Dyneema SK78 rope with a 4mm diameter and 28.6° for the Dyneema SK78 rope with a 22mm diameter.

We assume that the optimum bedding-in loading level is reached when the realignment of the strands towards the rope axis stops. The criterion to reach this optimum level, was chosen to be:

$$\left(\frac{d\alpha}{dF}\right)_{F_{opt}} = 0.05\left(\frac{d\alpha}{dF}\right)_{F=0}$$

Where α is the strand-strand angle and F is the tension load applied on the rope.

Thus the optimum bedding-in loading level is 32.0% of the MBL for the Dyneema SK99 rope with a 4mm diameter, 27.4% for the Dyneema SK78 rope with a 4mm diameter and 22.0% for the Dyneema SK78 rope with a 22mm diameter.

As shown previously, the influence of the bedding-in loading path is small. One load/unload cycle at the optimum loading level is sufficient to stabilize the mechanical properties of the rope.

iv. Maximal tensile strength

According to the experimental data, the maximal tensile strength from the highest to the lowest can be ranked as follows: 1/Filament, 2/Yarn and 3/Rope. This ranking is not surprising; previous studies have already observed stress concentrations in rope construction resulting in lower strength than their constituent yarns (Del Vecchio, 1992)(Lechat, 2007). The filament path in a rope is more complex than in a yarn, and results in stress concentrations between fibers. This phenomenon is sometimes called the bundle effect, and can explain why rope construction has a lower tensile strength than a yarn and a filament.

The BI procedures studied here do not weaken the rope even with a 50% MBL bedding-in load level. Previous studies have concluded that if the maximal bedding-in load does not exceed 60% of the MBL, fibers are not damaged (Francois and Davies, 2000). In addition an increase of 10% of the maximal tensile strength can be observed on the rope scale after BI. As demonstrated previously, the fibers tend to re-align in the tensile direction. The bedding-in protocol helps to organize the fibers along the neutral fiber

of the rope and the bundle effect is reduced. The maximal tensile strength is slightly higher for the filament than for the yarn. This observation is in agreement with the bundle effect.

b. Influence of the Load/Unload sequence BI protocol

Scale		Filament			Yarn			Rope		
Level of BI (% of the MBL)		10	30	50	10	30	50	10	30	50
Post-BI Strain	Without BI	/			/			/		
	With BI	0.17	0.4	0.7	1.01	1.25	1.41	1.84	2.56	2.97
	%	/	/	/	/	/	/	/	/	/
Maximal Strain	Without BI	4.7			3.53			4.74		
	With BI	4.57	3.57	3.43	2.7	2.72	2.82	3.91	3.1	3.13
	%	-3%	-24%	-27%	-23%	-23%	-20%	-17%	-35%	-34%
Maximal Stress	Without BI	3.16			2.86			1.67		
	With BI	3.24	3.52	3.14	2.56	2.72	2.85	1.82	1.82	1.83
	%	3%	11%	-1%	-10%	-5%	0%	9%	9%	10%

Table 4. Influence of LU bedding-in at different maximal BI loads for each rope scale

Table 4 compares the evolution of post-BI strain, maximal strain and maximal stress depending on the BI load level and the rope scale in the case of the Load/Unload sequence BI protocol. The post-BI strain increases with the BI load level and with higher scale as already observed previously.

The evolution of the maximal tensile stress seems stable in a range of 10% for the filament and yarn scale. The experimental noise is higher for the yarn and the filament than for the rope as shown by Figure 13.d. Therefore the results for yarn and for filament can be considered stable. The experimental noise for the maximal tensile stress I the rope is a lot lower, and shows a 10% increase of the maximal tensile stress for

the rope after BI. The reorganization of fibers during the BI of a rope decreases the bundle effect and increases the maximal tensile stress.

The maximum strain also seems to reach a maximum after a preload of 30% of the MBL. As observed earlier, the 'locking angle' between the strands is achieved with a 30% preload. This can explain the stabilization of the maximal strain for a preload level higher than 30% of the MBL.

Similar observations can be made for the 10 cycles Load/Unload and relaxation BI protocol.

Figure 21 shows how the rope stiffness changes for the different BI protocols.

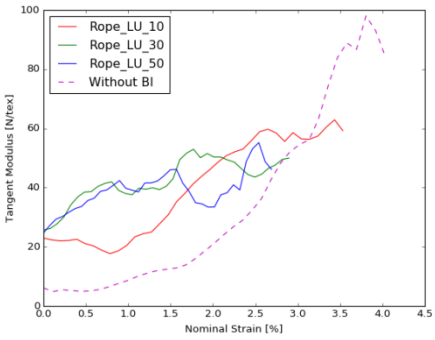

Figure 21.a. Change in tangent modulus for LU BI protocol

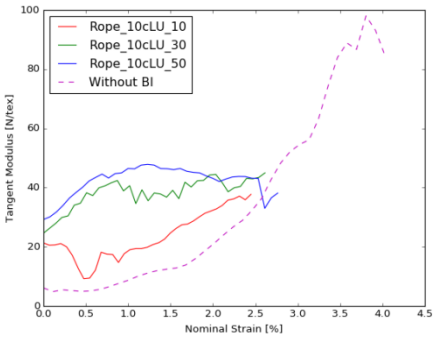

Figure 21.b. Change in tangent modulus for 10cLU BI protocol

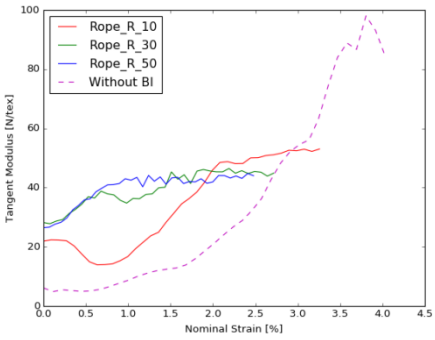

Figure 21.c. Change in tangent modulus for R BI protocol

The change in the tangent modulus with nominal strain is nonlinear without the BI protocol. With a 10% MBL BI protocol, the initial modulus is higher but still unstable. With 30% and 50 MBL BI protocols, the modulus is more stable than for lower BI load and the initial modulus is still around 30N/tex for both. Also the initial modulus is higher for the 30% and 50% preload levels than for 10%.

The modulus after a BI protocol seems to reach an optimum level. This optimum modulus is especially notable for the relaxation BI case, with a value around 60N/tex. But the tangent modulus does not seem to reach an optimum level for the case of rope without BI.

IV. Conclusion

This paper describes the influence of bedding-in loading on the mechanical performance of braided HMPE fiber rope developed for nautical applications. The results show that in order to improve rope properties significantly a preloading sequence should be applied, with loads at least to 30% of the break load. The loading path is of secondary importance. The improved rope behavior is the result of

contributions both at the fiber level (polymer molecule reorganization and alignment), and from the rope construction (alignment and compaction). The observation of the apparent diameter of a rope and the change in the strand orientation during a monotonous loading allow an optimum bedding-in load level to be determined rapidly. This was applied successfully to a larger braid, but it would be very interesting to extend this study to bigger ropes and different rope constructions.

These results are important, because a rope which has not been fully bedded-in may de-tension in service. This may have significant consequences on marine structures for example, a sailing boat mast may be less securely held or a floating offshore platform may require mooring line re-tensioning to limit the platform offset. For the latter, permanent removal of bedding-in strain can also significantly reduce the amount of steel chain required during take-up on winches.

V. References

American Bureau of Shipping (ABS), 2011. Guidance notes on the application of fiber ropes in the offshore mooring. ABS Press 29–40.

Banfield, S., Casey, N., 1998. Evaluation of fibre rope properties for offshore mooring. Ocean Eng. 25, 861–879.

Bureau Veritas, 2007. Certification of Fibre Ropes for Deepwater Offshore Services.

Casey, N.F., Banfield, S.J., 2005. OTC 17068 Factors Affecting the Measurement of Axial Stiffness of Polyester Deepwater Mooring Rope Under Sinusoidal Loading. Offshore Technol. Conf. 1–12.

Casey, N.F., Belshaw, R., Paton, A.G., Hooker, J., 2000. OTC 12177 Short- and Long-Term Property Behaviour of Polyester Rope. Offshore Technol. Conf. 1–12.

Chailleux, E., Davies, P., 2005. A Non-Linear Viscoelastic Viscoplastic Model for the Behaviour of Polyester Fibres. Mech. Time-Dependent Mater. 9, 147–160.

Costa, H.S., Chimisso, F.E.G., 2011. Modelling creep tests in HMPE fibres used in ultra-deep-sea mooring ropes. Int. J. Solids Struct. 48, 144–152. https://doi.org/10.1016/j.ijsolstr.2010.09.015

Davies, P., Bouquet, P., Conte, M., Deuff, A., 2006. OTC 17872 Tension / Torsion Behavior of Deepwater

Synthetic Mooring Lines. Offshore Technol. Conf. 1–8.

Davies, P., François, M., Veritas, B., Ifp, F.G., Baron, P., Engineering, D., Salomon, K., Offshore, B., Technip, D.T., 2002. OTC 14246 Synthetic Mooring Lines for Depths to 3000 Meters. Offshore Technol. Conf. 1–9.

Davies, P., Reaud, Y., Dussud, L., Woerther, P., 2011. Mechanical behaviour of HMPE and aramid fibre ropes for deep sea handling operations. Ocean Eng. 38, 2208–2214. https://doi.org/10.1016/j.oceaneng.2011.10.010

Del Vecchio, C.J.M., 1992. Light Weight Materials for Deep Water Moorings. PhD Thesis, University of Reading.

Fer, F., 1971. Thermodynamique macroscopique. Gordon Breach Sci. Publ.

Francois, M., Davies, P., 2000. Fibre rope deep water mooring: a practical model for the analysis of polyester mooring systems. Rio Oil Gas Conf.

Ghoreishi, S.R., 2005. Modelisation analytique et caracterisation experimentale du comportement de cables synthetiques. PhD Thesis, Ecole Centrale de Nantes.

Ghoreishi, S.R., Davies, P., Cartraud, P., Messager, T., 2007. Analytical modeling of synthetic fiber ropes. Part I: A linear elastic model for 1 + 6 fibrous structures. Int. J. Solids Struct. 44, 2943–2960. https://doi.org/10.1016/j.ijsolstr.2006.08.032

Hooker, J.., Bosman, R.L.M., 1999. Recent Investigation into the Physsical Properties of Superline Polyester Ropes. Prep. Present. Moorings Anchors Deep Ultra Deep Water Fields.

Hoppe, L.F.E., 1991. Modelling the static loading behavior of Dyneema in wire-rope construction. MTS RTM.

Humeau, C., 2017. Contribution to the study of coupling between moisture diffusion and mechanical stress, in high performance marine. PhD Thesis, Université de Nantes.

Humeau, C., Davies, P., Smeets, P., Engels, T.A.P., Govaert, L.E., Vlasblom, M., Jacquemin, F., 2018. Tension fatigue failure prediction for HMPE fi bre ropes. Polym. Test. 65, 497–504. https://doi.org/10.1016/j.polymertesting.2017.12.014

International Standards Organization (ISO), 2004. Fibre ropes for offshore station keeping — Polyester, ISO 18692.

Lechat, C., 2007. Comportement mécanique de fibres et d'assemblages de fibres en polyester pour cables d'amarrage de plates-formes offshore. PhD Thesis, Ecole des Mines de Paris.

Leech, C.M., 2003. The modelling and analysis of splices used in synthetic ropes. Proc. Math. Phys. Eng. Sci. 459, 1641–1659.

Leech, C.M., Hearle, J.W.S., 1993. Modelling Tension and Torque Properties of Fibre Ropes and splices. Int. Offshore Polar Eng. Conf. 6–11.

Lian, Y., Liu, H., Huang, W., Li, L., 2015. A creep – rupture model of synthetic fiber ropes for deepwater moorings based on thermodynamics. Appl. Ocean Res. 52, 234–244. https://doi.org/10.1016/j.apor.2015.06.009

Lian, Y., Liu, H., Li, L., Zhang, Y., 2018a. An experimental investigation on the bedding-in behavior of synthetic fi ber ropes. Ocean Eng. 160, 368–381. https://doi.org/10.1016/j.oceaneng.2018.04.071

Lian, Y., Liu, H., Yim, S.C., Zheng, J., Xu, P., 2019. An investigation on internal damping behavior of fiber rope. Ocean Eng. 182, 512–526. https://doi.org/10.1016/j.oceaneng.2019.04.087

Lian, Y., Zheng, J., Liu, H., Xu, P., Gan, L., 2018b. A study of the creep-rupture behavior of HMPE ropes using viscoelastic-viscoplastic-viscodamage modeling. Ocean Eng. 162, 43–54. https://doi.org/10.1016/j.oceaneng.2018.05.003

Liu, H., Huang, W., Lian, Y., Li, L., 2014. An experimental investigation on nonlinear behaviors of synthetic fiber ropes for deepwater moorings under cyclic loading. Appl. Ocean Res. 45, 22–32. https://doi.org/10.1016/j.apor.2013.12.003

Milne, K.A., Mclaren, A.J., 2006. An assessment of the strength of knots and splices used as eye terminations in a sailing environment. Department of Mechanical Engineering, University of Strathclyde, Glasgow, UK.

Raoof, M., Hobbs, R.E., 1988. Analysis of Multilayered Structural Strands. J. Eng. Mech. 114, 1166–1182.

Rawal, A., Sibal, A., Saraswat, H., Kumar, V., 2015. Geometrically controlled tensile response of braided sutures. Mater. Sci. Eng. C 48, 453–456. https://doi.org/10.1016/j.msec.2014.12.043

Vlasblom, M., 2018. 18 - The manufacture, properties, and applications of high-strength, high-modulus polyethylene fibers, Handbook of Properties of Textile and Technical Fibres. Elsevier Ltd. https://doi.org/10.1016/B978-0-08-101272-7.00018-3

Vu, T.D., Durville, D., Davies, P., 2015. Finite element simulation of the mechanical behavior of synthetic braided ropes and validation on a tensile test. Int. J. Solids Struct. 58, 106–116. https://doi.org/10.1016/j.ijsolstr.2014.12.022

Weller, S.D., Davies, P., Vickers, A.W., Johanning, L., 2014. Synthetic rope responses in the context of load history : Operational performance. Ocean Eng. 83, 111–124. https://doi.org/10.1016/j.oceaneng.2014.03.010

Williams, J.G., Ceac, H., Miyase, A., Ceac, H., Li, D., 2002. Small-Scale Testing of Damaged Synthetic Fiber Mooring Ropes. Offshore Technol. Conf. 1–13.